Double-diffusive instabilities in a vertical slot

By OLIVER S. KERR AND KIT YEE TANG

Department of Mathematics, City University, Northampton Square, London EC1V 0HB, UK

A fluid stably stratified by a salinity gradient and enclosed between two vertical boundaries can become unstable when it is subjected to a temperature difference between the walls. The linear stability of such a fluid in a vertical slot is investigated. Errors in earlier results are found, confirming recent results of Young & Rosner (1998). Four different asymptotic regimes on the stability boundary are identified. One of these, the limit of a strong salinity gradient, has previously been analysed. The analyses of the separate asymptotic limits of weak salinity gradient, large temperature difference and small wavenumber are also given. These four cases make up much of the total boundary between stability and instability for double-diffusive instabilities in a vertical slot, and so most of this boundary can be mapped out for general Prandtl numbers and salt/heat diffusivity ratios using these results.

1. Introduction

The term 'double-diffusive convection' applies to convection in a fluid where there are two diffusing components which have an effect on the buoyancy. The archetypal case is heat and salt. We will follow the usual convention of referring to the faster diffusing component in the fluid as 'heat' and the slower diffusing component as 'salt'. Convection that is dominated by the presence of two components is very common in geophysical systems and has been the subject of much study since Stern (1960) realized the important implication of an 'oceanographical curiosity' (Stommel, Arons & Blanchard 1956). A broad view of the subject of double-diffusive convection is given by Brandt & Fernando (1996).

The effect of horizontal temperature and salinity gradients on a stably stratified fluid was first examined by Stern (1967) in the context of fronts in the oceans. Thorpe, Hutt & Soulsby (1969) investigated the effect of lateral heating on a salt-stratified body of fluid in both narrow and wide vertical slots. Their investigation was both experimental and, under the assumption that the salinity gradient was strong, theoretical. The linear analysis in this limit was further investigated by Hart (1971) who also conducted a limited numerical investigation into the stability for a range of salt stratifications in a slot. Hart later went on to investigate some nonlinear aspects of double-diffusive convection in a vertical slot (Hart 1973). A more detailed examination of the linear stability of a salinity gradient in a vertical slot was conducted by Thangam, Zebib & Chen (1981). They calculated the criteria for the onset of instability for a large range of salinity gradients. However, for a relatively small range of gradients some of their results were erroneous. This was pointed out by Young & Rosner (1998), and is confirmed here. Young & Rosner calculated the stability boundary for several values of the salt/heat diffusivity ratio, and also conducted a weakly nonlinear analysis of these instabilities.

In this paper we shall again look at the linear stability of a salinity gradient in an infinite vertical slot. In §2 we will give the governing equations for the linear stability

of the fluid in a vertical slot. We shall present the results of numerical calculations of the stability boundary. These calculations were performed using two different numerical techniques, a shooting method and a Galerkin approach. We will identify four different sections of the stability boundary which are amenable to asymptotic analysis. One of these, the strong salinity gradient limit, was identified and analysed by Thorpe *et al.* In §3 we present the asymptotic analysis of each of these regimes. Finally, in §4, we will discuss the results.

2. Governing equations and marginal stability

We consider the linear stability of an infinite vertical slot which contains a body of fluid with a uniform vertical salinity gradient when there is a constant temperature difference imposed across the walls. We will assume the walls are impermeable to salt. We will follow previous authors and only consider two-dimensional instabilities. These have been shown to be the most unstable modes for at least some of the parameter ranges under consideration here (Thorpe *et al.* 1969).

In this section we will follow the formulation of Thangam *et al.* (1981) in their investigation of the stability of a salinity gradient in a vertical slot. We will use slightly different notations which will, we hope, lead to an improvement in clarity in the some of the asymptotic expansions used in the subsequent section. For further details of the derivation of these equations the reader is referred to this earlier paper.

The non-dimensional parameters for the heating on a salinity gradient in a slot are the temperature and salt Rayleigh numbers

$$Ra_T = \frac{g\alpha\Delta T D^3}{\nu\kappa_T}, \qquad Ra_S = \frac{g(-\beta\overline{S}_z)D^4}{\nu\kappa_T}, \tag{2.1}$$

and the Prandtl number and salt/heat diffusivity ratio

$$\sigma = \frac{\nu}{\kappa_T}, \qquad \tau = \frac{\kappa_S}{\kappa_T}. \tag{2.2}$$

Here g is the acceleration due to gravity, ν the kinematic viscosity, κ_T and κ_S the heat and salt diffusivities, α the coefficient of thermal expansion and β the coefficient of density increase with respect to the addition of salt. The walls are a distance D apart, with an imposed temperature difference of ΔT. The uniform vertical salinity gradient in the slot is $\overline{S}_z$. Since we are using the convention that the faster diffusing component is referred to as the temperature, the salt/heat diffusivity ratio, τ, is always less than 1.

If the governing equations are made non-dimensional using the scalings D for length, D^2/κ_T for time, ΔT for temperature and $D\left|\overline{S}_z\right|$ for salinity, then the steady non-dimensional background state is given by

$$\overline{W}(x) = \frac{Ra_T}{2M^3(\sin M + \sinh M)}\left(\sinh M_1 \sin M_2 - \sin M_1 \sinh M_2\right), \tag{2.3a}$$

$$\overline{T}(x) = -x, \tag{2.3b}$$

$$\overline{S}_x(x) = -\frac{Ra_T}{4\tau M^4}\left(1 + \frac{1}{\sin M + \sinh M}(\cosh M_1 \sin M_2 - \cosh M_2 \sin M_1\right.$$

$$\left. - \sinh M_1 \cos M_2 + \sinh M_2 \cos M_1)\right), \tag{2.3c}$$

where

$$M = \left(\frac{Ra_S}{4\tau}\right)^{1/4}, \qquad M_1 = \left(Mx + \frac{M}{2}\right), \qquad M_2 = \left(Mx - \frac{M}{2}\right). \qquad (2.4)$$

Here $\overline{W}(x)$, $\overline{T}(x)$ and $\overline{S}_x(x)$ are the non-dimensional vertical velocity, the temperature and the horizontal salinity gradient. These satisfy the boundary conditions

$$\overline{W}(\pm\tfrac{1}{2}) = 0, \qquad \overline{T}(\pm\tfrac{1}{2}) = \mp\tfrac{1}{2}, \qquad \overline{S}_x(\pm\tfrac{1}{2}) = 0. \qquad (2.5)$$

The coefficients in the equations for linear perturbations to this non-dimensional background state are independent of the non-dimensional time, t, and the vertical coordinate, z, and so we can consider perturbations which are proportional to $\exp(\lambda t + i\alpha z)$, where λ is the growth rate and α the vertical wave number. This leads to a set of linear equations for the perturbation stream function, temperature and salinity:

$$\left(\frac{d^2}{dx^2} - \alpha^2\right)^2 \psi - \frac{i\alpha}{\sigma}\left(\overline{W}(x)\left(\frac{d^2}{dx^2} - \alpha^2\right)\psi - \psi\overline{W}''(x)\right)$$
$$+ Ra_T T' - Ra_S S' - \frac{\lambda}{\sigma}\left(\frac{d^2}{dx^2} - \alpha^2\right)\psi = 0, \quad (2.6a)$$

$$\left(\frac{d^2}{dx^2} - \alpha^2\right)T + i\alpha\psi\overline{T}'(x) - i\alpha\overline{W}(x)T - \lambda T = 0, \qquad (2.6b)$$

$$\tau\left(\frac{d^2}{dx^2} - \alpha^2\right)S + i\alpha\psi\overline{S}'(x) - i\alpha\overline{W}(x)S + \psi' - \lambda S = 0, \qquad (2.6c)$$

with boundary conditions

$$\psi = \psi' = T = S' = 0 \quad \text{on} \quad x = \pm\tfrac{1}{2}. \qquad (2.7)$$

The above equations give an eigenvalue problem for the growth rate, λ, for any given set of parameters Ra_T, Ra_S, σ and τ. Throughout this paper we will consider the case of $\sigma = 6.7$ and $\tau = 0.01$, the approximate values for common salt in water.

We wish to find the marginal stability curve for this system of equations. This corresponds to the boundary in the (Ra_T, Ra_S)-plane which separates regions where solutions with a positive real part to their growth rate, λ, exist from regions where they do not. On this boundary there will usually be a solution for some value of the vertical wavenumber, α, with either $\lambda = 0$ or, if the onset of instability is oscillatory, with $\lambda = i\omega$ for some non-zero ω. The eigenvalues and solutions of these equations were calculated numerically. Originally a standard shooting method based around a fourth-order Runge–Kutta scheme was employed to investigate this stability boundary. However, when results were found which differed from those of Thangam *et al.* it was felt that confirmation should be found using an totally different numerical method. For this verification of the results we employed the Galerkin method of Thangam *et al.*, expanding the stream function, temperature and salinity using complete sets of orthogonal functions. For further details of this method see their paper. Taking a truncation after N terms of each of these series results in a $3N \times 3N$ matrix eigenvalue problem which was solved numerically using NAG library routines. The choice of the truncation level, N, depended on which part of the stability boundary was being considered.

The second numerical scheme proved to be more robust as it was able to calculate solutions in the case of small salinity gradient where the shooting method was
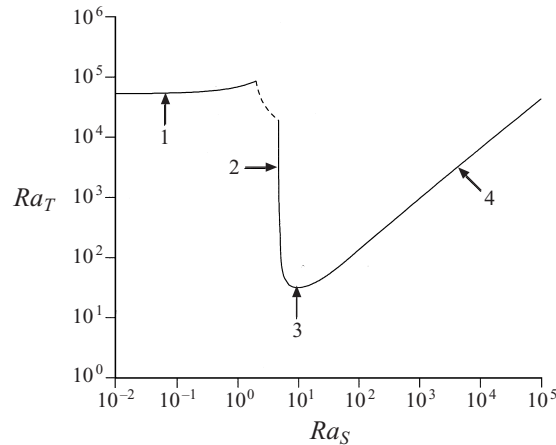
FIGURE 1. Marginal stability curve for a salinity gradient in a vertical slot with $\sigma = 6.7$ and $\tau = 0.01$. The onset of instability is steady everywhere except for the dashed curve. The numbers indicate the sections of the curve where different asymptotic regimes hold.

unable to find solutions. Unfortunately the solutions found were not always very accurate unless a sufficiently large N was used (see the Appendix). The reason for the failure of the shooting method in this region will become clear in the discussion of the asymptotics of this regime in § 3.1. In regimes where both schemes produced results the agreement was always to at least five significant figures, and usually better than this.

The full stability boundary is shown in figure 1. For values of Ra_S greater than 10 and less that 0.45 the curve is essentially the same as that of Thangam *et al.* These authors found that all modes of instability were oscillatory between these two limits. However, the results found here are very different. The part of the stability boundary below $Ra_S = 0.45$ representing steady convection continues past this point, curving upwards. The instabilities do not become oscillatory until $Ra_S = 2.0256$. There is then a small region when Ra_S lies between 2.0256 and 4.7703 where the initial instability is oscillatory. This is shown in the figure by the dashed line. Along this branch of solutions the frequency decreases from around 235 to 115. At the end of this oscillatory branch, where $Ra_T = 18\,767$, the preferred mode of instability again becomes steady. The next part of the boundary is almost vertical and sweeps down to a minimum near $Ra_S = 10$, and then increases steadily as Ra_S increases.

Thus, most of the oscillatory solutions reported by Thangam *et al.* for Ra_S between 0.45 and 10 are not found here. The only part of the boundary where the initial instability is oscillatory is along the small portion of the boundary indicated by the dashed line in figure 1. These oscillatory solutions continue into the unstable region as a local maximum in the growth rate, however no oscillatory solutions were found for Ra_T much below 12 000. These corrected results have also been found recently by Young & Rosner (1998) for slightly different parameters.

The wavenumbers, α, corresponding to the points of marginal stability are shown in figure 2. Due to the shape of the boundary these are shown in two parts. The first, figure 2(*a*), shows α as a function of Ra_S. Below $Ra_S = 2.0256$ the wave number is approximately that of the primary instability in a vertical slot in the absence of any salinity gradient, but showing a slight decrease in the wavenumber as the salt Rayleigh number increases. At $Ra_S = 2.0256$ there is a jump in the value associated with the transition to the oscillatory branch of instabilities, shown as a dashed line.
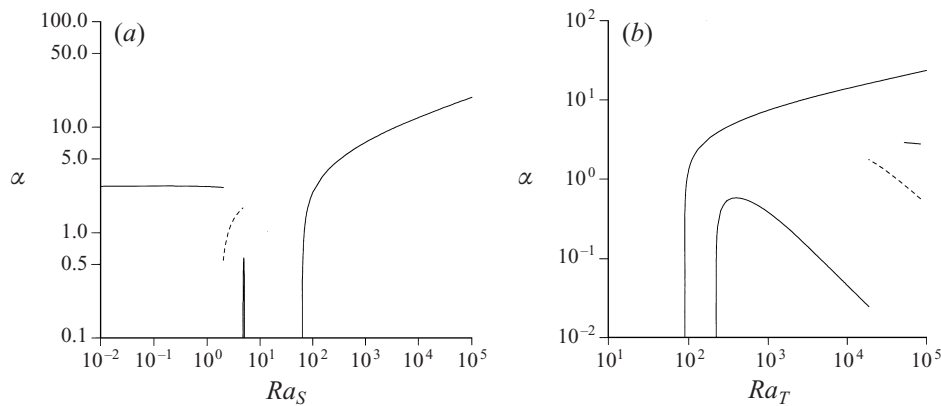
FIGURE 2. The vertical wavenumber for the disturbances at the onset of instability as a function of (*a*) Ra_S and (*b*) Ra_T.

This branch shows a steady increase until $Ra_S = 4.7703$ where there is a another jump back to a steady branch of solutions. This branch shows a sharp peak whose details are lost here due to stability boundary being almost parallel to the Ra_T-axis. The wavenumber α varies significantly in this region, and so large changes to α occur over a limited range of Ra_S. After this peak the wavenumber drops away sharply. Between $Ra_S = 5.044$ and $Ra_S = 63.4$ the vertical wavenumber of the most unstable solutions above the stability boundary approaches zero as the boundary is approached, and so this part of the boundary could be considered to have $\alpha = 0$. Strictly speaking solutions do not exist with this value, and so states with zero growth rate do not exist on this part of the boundary.

The details of the peak in figure 2(*a*) are revealed in figure 2(*b*). This shows α as a function of Ra_T. The upper curve gives the large Ra_S behaviour seen previously. The short segments of solid line and dashed line to the right give the small-Ra_S and oscillatory branches of solutions respectively. These parts of the curve were clearly visible in figure 2(*a*). The last curve corresponds to the almost vertical section of the stability boundary in figure 1. This shows the rise in α from the $\alpha = 0$ part of the curve to a peak, and its subsequent decline in an almost straight line with slope -1 until the transition to the oscillatory branch of solutions is reached at $Ra_T = 18\,767$.

Four sections of the marginal stability curve in figure 1 have been numbered. These correspond to the four asymptotic regimes that are investigated in the next Section. The first is the small-salinity-gradient regime where the presence of the salinity gradient perturbs the stability result for the lateral heating of a vertical slot. The second regime, which corresponds to the vertical section of the curve, is where the onset of instabilities is essentially independent of the temperature difference across the slot. The third regime corresponds to the curved part at the bottom of the stability curve where $\alpha = 0$. The last region corresponds to the case where the salinity gradient is strong. This last region was first analysed by Thorpe *et al.* (1969).

3. Asymptotic regimes

In this Section we look at the four numbered sections of the marginal stability curve in figure 1, each corresponding to a part which is amenable to asymptotic analysis. The first is the small-Ra_S regime where the presence of the weak salinity gradient perturbs

the stability result for the lateral heating of a vertical slot in the absence of any salinity gradients. The second regime corresponds to the upper portion of the vertical section of the curve, where the onset of instabilities is essentially independent of the temperature difference. This branch of solutions ceases to be a global maximum in the growth rate when Ra_T exceeds 18 767 where the oscillatory mode of instability takes over. However it continues to be a local maximum and can be traced well into the region of instability. The analysis of this branch corresponds to taking the large-Ra_T limit. The third regime corresponds to the curved part at the bottom of the stability curve where the vertical wavelength of the instabilities tends to infinity. To find the location of this boundary we look at the limit as α tends to zero. This is the region that gives the minimum temperature difference across the slot that can destabilize a salinity gradient for our chosen parameters. For other parameters this may not be the case; however it will provide an upper bound for such a minimum temperature difference. We shall see that this temperature difference is, in general, several orders of magnitude less than that required to destabilize an unstratified fluid between vertical walls. The last region is where the strong salinity gradient dominates the instabilities. This corresponds to taking the large-Ra_S limit and was first investigated by Thorpe *et al.* (1969).

The four regimes are examined in the following subsections. In each case the onset of instability is to non-oscillatory modes, so we can restrict ourselves to considering the case $\lambda = 0$ in this Section.

In order to avoid a proliferation of different notations some expressions used in different subsections may be repeated. Definitions of new variables or functions in each subsection should be considered to apply to that subsection only.

3.1. *Small salinity gradient*

The first section of the stability curve that we will examine (numbered 1 in figure 1) corresponds to the case where there is a weak salinity gradient that perturbs what is essentially the thermally driven problem of a laterally heated vertical slot that has been examined by many authors since Batchelor (1954). For Prandtl numbers less than 12.7 (Korpela, Gözüm & Baxi 1973) the initial instability takes the form of stationary convection cells as is found here (Vest & Arpaci 1969). For larger Prandtl numbers the initial instabilities take the form of travelling waves. The analysis here assumes that the former steady mode of instability is the relevant one.

We assume that the salt Rayleigh number, Ra_S, is small and pose the asymptotic expansions

$$\psi(x) = \psi_0(x) + Ra_S \psi_1(x) + \cdots, \tag{3.1a}$$

$$T(x) = T_0(x) + Ra_S T_1(x) + \cdots, \tag{3.1b}$$

$$S(x) = S_0(x) + Ra_S S_1(x) + \cdots, \tag{3.1c}$$

with

$$Ra_T = Ra_{T0} + Ra_S Ra_{T1} + Ra_S^2 Ra_{T2} + \cdots. \tag{3.1d}$$

The background velocity and salinity profiles can also be expanded in asymptotic series:

$$\overline{W}(x) = Ra_T(\overline{W}_0(x) + Ra_S \overline{W}_1(x) + \cdots), \tag{3.2a}$$

$$\overline{S}(x) = Ra_T(\overline{S}_0(x) + Ra_S \overline{S}_1(x) + \cdots), \tag{3.2b}$$

where

$$\overline{W}_0(x) = x(4x^2 - 1)/24, \tag{3.3a}$$

$$\overline{W}_1(x) = -x(4x^2 - 1)(16x^4 - 24x^2 + 29)/(322\,560\tau), \qquad (3.3b)$$

$$\overline{S}_0(x) = -(4x^2 - 1)^2/(384\tau), \qquad (3.3c)$$

$$\overline{S}_1(x) = (48x^4 - 88x^2 + 163)(4x^2 - 1)^2/(30\,965\,760\tau^2), \qquad (3.3d)$$

The leading-order velocity is that which would be found in the absence of a vertical salinity gradient.

The leading-order perturbation equations are

$$\left(\frac{\mathrm{d}^2}{\mathrm{d}x^2} - \alpha^2\right)^2 \psi_0 - \frac{\mathrm{i}\alpha}{\sigma}\left(Ra_{T0}\overline{W}_0(x)\left(\frac{\mathrm{d}^2}{\mathrm{d}x^2} - \alpha^2\right)\psi_0 - \psi_0 Ra_{T0}\overline{W}_0''(x)\right)$$
$$+ Ra_{T0}T_0' = 0, \qquad (3.4a)$$

$$\left(\frac{\mathrm{d}^2}{\mathrm{d}x^2} - \alpha^2\right)T_0 - \mathrm{i}\alpha\psi_0 - \mathrm{i}\alpha Ra_{T0}\overline{W}_0(x)T_0 = 0, \qquad (3.4b)$$

$$\left(\frac{\mathrm{d}^2}{\mathrm{d}x^2} - \alpha^2\right)S_0 + \frac{\mathrm{i}\alpha\psi_0 Ra_{T0}\overline{S}_0'(x)}{\tau} - \frac{\mathrm{i}\alpha Ra_{T0}\overline{W}_0(x)}{\tau}S_0 + \psi_0'/\tau = 0, \qquad (3.4c)$$

with boundary conditions

$$\psi_0 = \psi_0' = T_0 = S_0' = 0 \quad \text{on} \quad x = \pm\tfrac{1}{2}. \qquad (3.5)$$

It can be seen that the stream function and temperature equations are independent of the salinity equation. This pair of equations is just that of the laterally heated unstratified slot. These can be solved numerically and yield the leading-order condition for the onset of instability for Prandtl number $\sigma = 6.7$:

$$Ra_{T0} = 52\,715, \qquad \alpha = 2.7671. \qquad (3.6)$$

This is close to the result of Vest & Arpaci who found that the Rayleigh number at the onset of steady instabilities can be approximated by

$$Ra_T/\sigma \approx 7880. \qquad (3.7)$$

This result holds to within a few percent for a large range of Prandtl numbers.

The salinity equation can now, in principle, be solved. However, examination of the magnitude of some of the terms in (3.4c) shows that it is not a straightforward matter to solve this equation numerically. The problem comes from the factor $\mathrm{i}\alpha Ra_{T0}\overline{W}_0/\tau$. This has a magnitude that varies from 0 at the walls and in the centre to peaks of around 117 000. This results in the equations being very stiff, and with boundary layer behaviour in the centre of the slot where $\overline{W}_0$ vanishes as well as at the walls. This stiff behaviour was the cause of the original approach to solving the full system of equations using a shooting method failing along this branch of solutions.

The approach taken here to find a solution to the salinity equation is to exploit the large magnitude of the troublesome term. This enables us to find an approximate solution by a matched asymptotic expansion. The structure of the solution consists of outer solutions away from the walls and the centre, and inner boundary layer solutions at the walls and in the centre. Of these boundary layers, the one at the centre of the slot is the most important as this is the location of the sharp maximum in the salinity perturbation. The details of this asymptotic analysis are given in the Appendix.

To find the next-order perturbation for the thermal Rayleigh number a solvability condition is applied to the $O(Ra_S)$ equations for the stream function and temperature.

These equation are

$$\left(\frac{\mathrm{d}^2}{\mathrm{d}x^2} - \alpha^2\right)^2 \psi_1 - \frac{\mathrm{i}\alpha}{\sigma}\left(Ra_{T0}\overline{W}_0\left(\frac{\mathrm{d}^2}{\mathrm{d}x^2} - \alpha^2\right)\psi_1 - \psi_1 Ra_{T0}\overline{W}_0''\right) + Ra_{T0}T_1'$$

$$= \frac{\mathrm{i}\alpha}{\sigma}\left((Ra_{T0}\overline{W}_1 + Ra_{T1}\overline{W}_0)\left(\frac{\mathrm{d}^2}{\mathrm{d}x^2} - \alpha^2\right)\psi_0\right.$$

$$\left. -\psi_0(Ra_{T0}\overline{W}_1'' + Ra_{T1}\overline{W}_0'')\right) - Ra_{T1}T_0' + S_0', \quad (3.8a)$$

$$\left(\frac{\mathrm{d}^2}{\mathrm{d}x^2} - \alpha^2\right)T_1 - \mathrm{i}\alpha\psi_1 - \mathrm{i}\alpha Ra_{T0}\overline{W}_0 T_1 = \mathrm{i}\alpha\left(Ra_{T0}\overline{W}_1 + Ra_{T1}\overline{W}_0\right)T_0, \quad (3.8b)$$

with boundary conditions

$$\psi_1 = \psi_1' = T_1 = 0 \quad \text{on} \quad x = \pm\tfrac{1}{2}. \tag{3.9}$$

We multiply these equations by the complex conjugates of the adjoints of $\psi_0(x)$ and $T_0(x)$, $\hat{\psi}_0^*$ and $\hat{T}_0^*$ respectively, and integrate their sum over the slot to obtain a solvability condition for the existence of a steady solution:

$$\int_{-1/2}^{1/2}\left(\left(\left(\frac{\mathrm{i}\alpha}{\sigma}\left((Ra_{T0}\overline{W}_1 + Ra_{T1}\overline{W}_0)\left(\frac{\mathrm{d}^2}{\mathrm{d}x^2} - \alpha^2\right)\psi_0 - \psi_0(Ra_{T0}\overline{W}_1'' + Ra_{T1}\overline{W}_0'')\right)\right.\right.$$

$$\left.\left. -Ra_{T1}T_0' + S_0'\right)\hat{\psi}_0^* + \mathrm{i}\alpha\left(Ra_{T0}\overline{W}_1 + Ra_{T1}\overline{W}_0\right)T_0\hat{T}_0^*\right)\mathrm{d}x = 0. \quad (3.10)$$

This can be rearranged to give an expression for Ra_{T1} which can be evaluated numerically. This gives

$$Ra_{T1} = 13\,887. \tag{3.11}$$

This result is for a fixed value of the vertical wavenumber α corresponding to the minimum value of Ra_{T0}. the critical value of α will also vary with the leading-order perturbation being proportional to Ra_S. This has an effect on the critical value of Ra_T at $O(Ra_S^2)$ which is beyond the scope of the analysis presented here. This leading-order perturbation on the wavenumber can be found by expanding Ra_{T0} and Ra_{T1} in Taylor series around the critical value of the wavenumber for the heated slot problem. This gives the critical value of α as

$$\alpha = \alpha_0 - Ra_S\left(\frac{\partial^2 Ra_{T0}(\alpha_0)/\partial\alpha^2}{\partial Ra_{T1}(\alpha_0)/\partial\alpha}\right) + \cdots. \tag{3.12}$$

These derivatives were estimated, giving

$$\alpha \approx 2.7671 - 0.0525 Ra_S. \tag{3.13}$$

The above estimates were all made using solutions calculated using the shooting method based on the Runge–Kutta technique. Estimates of the leading-order perturbation to the temperature Rayleigh number based around the full numerical results obtained using the Galerkin approach are shown in table 1. This shows that a good estimate of Ra_{T0} was provided for all levels of the truncation. However the estimate for Ra_{T1} is quite poor for $N = 24$, and still not very good for $N = 48$. There is good agreement when the truncation is set to $N = 72$ and $N = 96$. This may be anticipated since the leading-order behaviour is just that of the heated slot with no effect of the

N	$Ra_S = 1.0$	$Ra_S = 0.1$	$Ra_S = 0.01$	$Ra_S = 0.001$	Ra_{T0}	Ra_{T1}
24	57 979.172	53 288.817	52 773.197	52 721.124	52 715.338	5 785.872
48	66 665.399	54 052.185	52 848.487	52 728.680	52 715.368	13 311.849
72	67 255.831	54 093.822	52 852.502	52 729.080	52 715.367	13 713.527
96	67 255.932	54 093.828	52 852.503	52 729.080	52 715.366	13 713.722

TABLE 1. Critical thermal Rayleigh numbers, Ra_T, for different salt Rayleigh numbers, Ra_S and truncation levels, N. Also included are the estimates of Ra_{T0} and Ra_{T1} based on the results for $Ra_S = 0.01$ and 0.001.
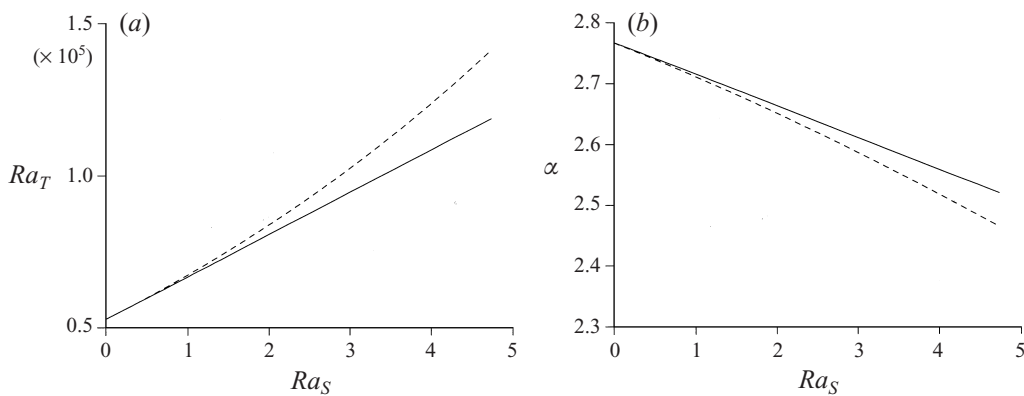

FIGURE 3. A comparison of the asymptotic behaviour (solid line) and the full numerical calculations (dashed line) for the small-Ra_S limit: (a) the critical value of Ra_T and (b) the corresponding vertical wavenumber, α.

salt. This problem has no boundary layer behaviour and is well resolved by all levels of truncation used here. To model the first-order perturbation requires a satisfactory solution of the salinity equation which requires a higher truncation level. The lack of accuracy for lower truncations is shown in the Appendix. For these larger values of N the expansion of the salinity has sufficient resolution near the centre of the slot to adequately resolve the boundary layer with its large peak. However for even larger values of Ra_S even when the truncation is set to $N = 72$ the resolution not adequate along this branch. Fortunately the expansion scheme chosen by Thangam *et al.*, and used here, has essentially uniform resolution across the whole slot, and does not concentrate the resolution near the boundaries as would be the case if, say, Chebyshev polynomials had been used. However, Chebyshev polynomials will probably be better in other regimes where the only thin boundary layers that need to be resolved are located at the walls.

A comparison of the asymptotic results and the full results found using the Galerkin method is shown in figure 3. Figure 3(a) shows the good agreement between the asymptotic results and the full results for small Ra_S. The oscillatory mode of instability becomes dominant for Ra_S just over 2; however this branch of solutions can still be traced as a local maximum in the growth rate for higher values of the salt Rayleigh number, and these values are shown here. The agreement between the asymptotics and the full numerical results for the critical wave number is shown in figure 3(b).

3.2. *Large temperature difference*

This branch of solutions (numbered 2 in figure 1) is characterized by an almost constant $O(1)$ value of the salt Rayleigh number, and a wavenumber that decays as Ra_T^{-1} as Ra_T increases. The full numerical solution indicates that this branch of solutions exists as a local maximum in the growth rate for Ra_T far beyond the point where the oscillatory mode of oscillation becomes dominant. We can exploit this by posing a large-Ra_T expansion for steady solutions:

$$\psi(x) = \psi_0(x) + Ra_T^{-1}\psi_1(x) + \cdots, \tag{3.14a}$$

$$T(x) = Ra_T^{-1}T_0(x) + Ra_T^{-2}T_1(x) + \cdots, \tag{3.14b}$$

$$S(x) = S_0(x) + Ra_T^{-1}S_1(x) + \cdots, \tag{3.14c}$$

$$Ra_S = Ra_{S0} + Ra_T^{-1}Ra_{S1} + \cdots. \tag{3.14d}$$

Noting that $\overline{W}(x)$ and $\overline{S}_x(x)$ are both proportional to Ra_T we will rewrite them as

$$\overline{W}(x) = Ra_T\overline{W}_0(x), \qquad \overline{S}_x(x) = Ra_T\overline{S}_{x0}(x)/\tau, \tag{3.15}$$

so that $\overline{W}_0(x)$ and $\overline{S}_{x0}(x)$ are functions of x and $M = (Ra_S/\tau)^{1/4}$ only. Rescaling the vertical wavenumber, $\alpha = Ra_T^{-1}\alpha_0$, gives the following leading-order set of equations:

$$\psi_0'''' - \frac{i\alpha_0}{\sigma}\left(\overline{W}_0(x)\psi_0'' - \psi_0\overline{W}_0''(x)\right) + T_0' - Ra_{S0}S_0' = 0, \tag{3.16a}$$

$$T_0'' - i\alpha_0\psi_0 - i\alpha_0\overline{W}_0(x)T_0 = 0, \tag{3.16b}$$

$$\tau S_0'' + i\alpha_0\psi_0\overline{S}_{x0}(x)/\tau - i\alpha_0\overline{W}_0(x)S_0 + \psi_0' = 0, \tag{3.16c}$$

with boundary conditions

$$\psi_0 = \psi_0' = T_0 = S_0' = 0 \quad \text{on} \quad x = \pm\tfrac{1}{2}. \tag{3.17}$$

These equations are not significantly simpler to solve than the full equations, except that Ra_T does not appear explicitly. These can be solved numerically in the same way as the full equations, and a minimum value of Ra_{S0} found with a corresponding value of α_0. For $\sigma = 6.7$ and $\tau = 0.01$ this point was found to occur at

$$Ra_{S0} = 4.7701, \qquad \alpha_0 = 442.66. \tag{3.18}$$

The comparison of this result with the full numerical results is shown in figure 4. This shows good agreement for both the salt Rayleigh number and the wavenumber, with the asymptotic results and the full numerical results being indistinguishable for Ra_T much above 3000. This corresponds to the upper portion of the vertical boundary in figure 1. Note that this branch of solutions can be followed some considerable distance into the region of global instability. The above scalings show that no singularities develop in these equations near this point as $Ra_T \to \infty$ as was the case in the previous asymptotic regime. Thus no particular difficulties are found in solving the full problem along this branch of solutions.

The above equations involve both σ and τ, and so in general the asymptotic behaviour for this branch has to be recalculated every time a different fluid and/or a different salt is used. However we can make a further simplification if we assume that the salt/heat diffusivity ratio, τ, is small. As $\tau \to 0$ we find that the appropriate scalings are $\psi_0 = O(1)$, $S = O(\tau^{-1})$, $Ra_S = O(\tau)$, $T_0 = O(\tau)$ and $\alpha_0 = O(\tau)$. If we define
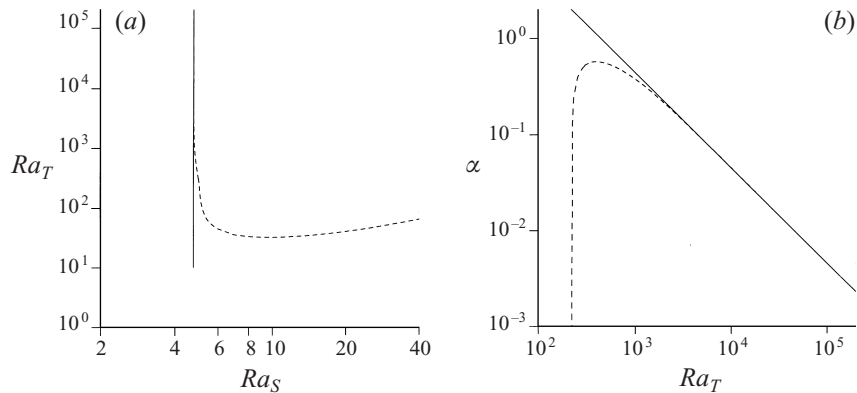
FIGURE 4. A comparison of the asymptotic behaviour (solid line) and the full numerical calculations (dashed line) for the large-Ra_T limit: (*a*) the vertical asymptote at $Ra_S = 4.7701$ and (*b*) the vertical wavenumber, α, as a function of Ra_T.

the new variables

$$\psi_0 = \psi^*, \qquad S_0 = \tau^{-1} S^*, \qquad Ra_{S0} = \tau Ra_S^*, \qquad T_0 = \tau T^*, \qquad \alpha_0 = \tau \alpha^*, \qquad (3.19)$$

then the leading set of equations is

$$\psi^{*''''} - Ra_S^* S^{*'} = 0, \qquad (3.20a)$$

$$T^{*''} - i\alpha^* \psi^* = 0, \qquad (3.20b)$$

$$S^{*''} + i\alpha^* \psi^* \overline{S}_{x0}(x) - i\alpha^* \overline{W}_0(x) S^* + \psi^{*'} = 0, \qquad (3.20c)$$

with boundary conditions

$$\psi^* = \psi^{*'} = T^* = S^{*'} = 0 \quad \text{on} \quad x = \pm\tfrac{1}{2}. \qquad (3.21)$$

The parameters σ and τ no longer appear in these leading-order equation. In order to find the relationship between Ra_S^* and α^* we only need to solve (3.20a) and (3.20c) simultaneously. The results are shown in figure 5. This shows Ra_S^* decreasing from a maximum of 501.36 at the origin towards an asymptote estimated to be at $Ra_S^* = 444.8$. We will return to this maximum value in the following Section. Although we have a minimum for Ra_S^* we no longer have a corresponding wavenumber.

Care must be taken in interpreting the above results for the limit $\tau \to 0$, especially looking at the large-α^* behaviour in figure 5. In order to derive the original large-Ra_T equations (3.16a)–(3.16c) we have used one limiting process which made some assumptions about the relative magnitudes of the terms in the full governing equations. In taking the second limiting process of $\tau \to 0$ we are making some additional assumptions which are compatible with the first, in that neglected small terms under the large-Ra_T assumption do not become large again under the small-τ assumption. However this is not the case if one then tries to take the further limit $\alpha^* \to \infty$. This is incompatible with the earlier assumptions that $\alpha \to 0$ as $Ra_T \to \infty$ and $\alpha^* \to 0$ as $\tau \to 0$. The original assumptions will always provide a constraint on the maximum allowable size of α^*. Thus the limit $Ra_S^* \to 444.8$ may only be approached for extreme values of Ra_T and τ. However, what this limit does provide is a lower bound for the possible minimum values of Ra_S^* in this asymptotic regime. It will be seen in the next subsection that this is a useful lower bound in that it is not too different in magnitude from an upper bound for the value of Ra_S on the stability boundary in this region.
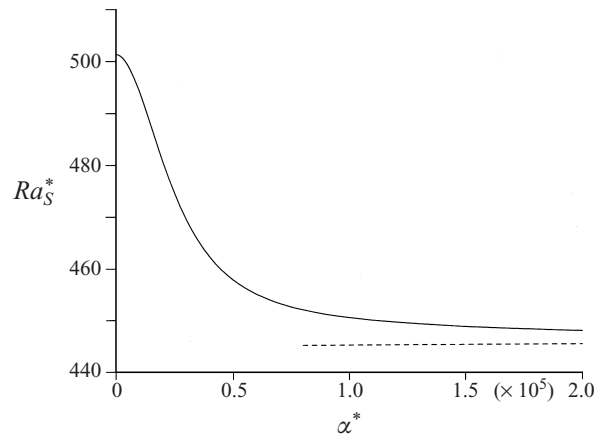
FIGURE 5. A graph of Ra_S^* as a function of α, with the large-α^* asymptote with $Ra_S^* = 444.8$ shown as a dashed line.

The most noticeable aspect of this large-Ra_T regime is the vertical nature of the stability boundary in the (Ra_T, Ra_S)-plane. This means that, for a given salinity gradient, increasing or decreasing the temperature difference across the slot has no effect on the stability of the fluid. This may, at first, seem bit surprising. Both $\overline{W}(x)$ and $\overline{S}_x(x)$ are proportional to Ra_T and hence the temperature difference. Thus the shear and the horizontal salinity gradient vary greatly along this branch of solutions. Both the shear of this background flow and the horizontal salinity gradients are potential sources of the instability mechanism, but since doubling both leads to little change in the stability one may conclude that one is a destabilizing effect and the other stabilizing, with the increase in one neutralizing the effect of the increase in the other. This can be confirmed by artificially multiplying either $\overline{W}_0(x)$ or $\overline{S}_{x0}(x)$ by some arbitrary factor in (3.16a)–(3.16c) and investigating the effect on the stability boundary. It is found that increasing the background velocity stabilizes the flow, while increasing the salinity gradient destabilizes the flow. If both are increased by the same factor there is little change in the stability. Thus we conclude that the driving force behind these instabilities is the horizontal salinity gradient, and the vertical shear is a stabilizing effect. This tendency for shear to suppress convection has been noted before in the context of double-diffusive convection by Linden (1974) in his investigation of the effect of shear on salt fingers.

For a salt/heat diffusivity ratio of 0.01 this asymptotic regime corresponds to the upper portion of the vertical branch labelled 2 in figure 1. From the above analysis we see that for smaller diffusivity ratios this region of validity will expand downwards. We shall see in the next Section that the lowest portion of the vertical boundary falls under a different asymptotic regime.

3.3. *Small wavenumber*

In this region (numbered 3 in figure 1) the marginal stability is governed by the behaviour of the governing equations in the limit $\alpha \to 0$. As mentioned in the previous section, there are no solutions to the perturbation equations when $\alpha = 0$. On first inspection it may seem that the appropriate balances for this limit are that $\psi = O(1)$, $T = O(\alpha)$ and $S = O(1)$. This scaling leads to a set of equations which does not have a solution. With this scaling S appears in the leading-order equations only in terms of its first and second derivatives. The no-flux boundary conditions for the

salinity allows arbitrary constants to be added to S in these simplified equations. If this constant term is $O(\alpha^{-1})$ then an extra term appears in the $O(1)$ equations which enables a solution to be found. Thus we pose an expansion

$$\psi(x) = \psi_0(x) + \alpha\psi_1(x) + \cdots, \qquad (3.22a)$$

$$T(x) = \alpha T_1(x) + \cdots, \qquad (3.22b)$$

$$S(x) = \alpha^{-1} S_{-1} + S_0(x) + \alpha S_1(x) + \cdots, \qquad (3.22c)$$

with S_{-1} constant. This expansion yields the leading-order equations

$$\psi_0'''' - Ra_S S_0' = 0, \qquad (3.23a)$$

$$T_1'' - i\psi_0 = 0, \qquad (3.23b)$$

$$\tau S_0'' + \psi_0' = i\overline{W}(x)S_{-1}, \qquad (3.23c)$$

with boundary conditions

$$\psi_0 = \psi_0' = T_1 = S_0' = 0 \quad \text{on} \quad x = \pm\tfrac{1}{2}. \qquad (3.24)$$

These equations can be solved explicitly to give solutions of the form

$$\psi_0(x) = iS_{-1} Ra_T f(x; M), \quad T_1 = S_{-1} Ra_T g(x; M), \quad S_0 = \frac{iS_{-1} Ra_T}{\tau} h(x; M), \quad (3.25)$$

where each of the real functions $f(x; M)$, $g(x; M)$ and $h(x; M)$ only depends on the various parameters through $M = (Ra_S/4\tau)^{1/4}$. The exact form of these expressions is lengthy and not very illuminating, and so have not been included here. Copies can be obtained from the Editorial Office of the *Journal of Fluid Mechanics*. We can write the background vertical velocity and horizontal salinity gradients in a similar fashion:

$$\overline{W}(x) = Ra_T \overline{W}^*(x; M), \qquad \overline{S}_x = \frac{Ra_T}{\tau}\overline{S}_x^*(x; M), \qquad (3.26)$$

where $\overline{W}^*$ and $\overline{S}_x^*$ only depend on x and M.

In order to derive a relation between Ra_T and Ra_S we need only look at the second-order salinity equation:

$$\tau S_1'' + \psi_1' = -i\overline{S}_x \psi_0 + i\overline{W}(x)S_0 + \tau S_{-1}. \qquad (3.27)$$

If we integrate this over the width of the slot then we obtain

$$\int_{-1/2}^{1/2} \tau S_1'' + \psi_1' \, dx = \int_{-1/2}^{1/2} -i\overline{S}_x \psi_0 + i\overline{W}(x)S_0 + \tau S_{-1} \, dx. \qquad (3.28)$$

The boundary conditions on S and ψ ensure that the integral on the left of this equation is identically zero. Rearranging the remaining terms gives

$$Ra_T = \tau \left(\int_{-1/2}^{1/2} -f(x; M)\overline{S}_x^*(x; M) + h(x; M)\overline{W}^*(x; M) \, dx \right)^{-1/2}. \qquad (3.29)$$

This integral inside the brackets does not involve any of the parameters of the problem except through M. It too can be evaluated explicitly, yielding another lengthy expression which again is not included here, but copies are available from the Editorial Office of the *Journal of Fluid Mechanics*.

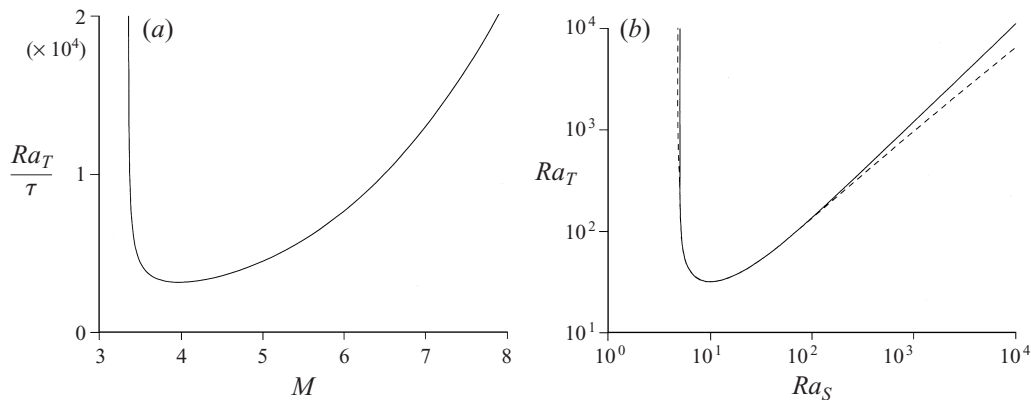The graph of Ra_T/τ as a function of M is shown in figure 6(a). The minimum

FIGURE 6. Graphs of (a) the value of Ra_T/τ at marginal stability as a function of M in the limit $\alpha \to 0$ and (b) the corresponding curve of Ra_T as a function of Ra_S (solid line) with a comparison with the stability boundary for the full problem (dashed line).

value can be found numerically, giving the minimum point on the marginal stability curve in the limit of small α

$$Ra_T/\tau = 3\,137.9, \qquad M = 3.9779. \qquad (3.30)$$

This value of M corresponds to a salt Rayleigh number of

$$Ra_S = 1\,001.6\tau. \qquad (3.31)$$

The left-hand branch has a vertical asymptote when the term in the brackets in (3.29) is zero. This occurs when $M = 3.3460$ or equivalently $Ra_S = 501.36\tau$. This is the same value as was found for the maximum of the curve in figure 5, although the value here does not require the assumption $\tau \to 0$ made in that part of the analysis of the previous subsection. The stability boundary obtained in the previous subsection for $\sigma = 6.7$ and $\tau = 0.01$ is lower than this value. Other choices of σ and τ will give different results for the position of the vertical portion of the stability boundary, but it can never lie to the right of the line found here. Thus this value of Ra_S gives an upper bound to the left-hand vertical part of the stability boundary. For small salt/heat diffusivity ratios the lower bound for Ra_S on this part of the stability boundary found in the previous subsection has a value of just under 90% of the value of the upper bound found here; thus the two results provide reasonably close limits on the position of the vertical portion of the stability boundary in the small-τ limit.

The stability boundary of the full problem is superimposed on the small-α asymptotic results in figure 6(b). The results show agreement around the bottom of the curve.

One feature of this asymptotic regime is that the temperature perturbation plays absolutely no part in the analysis of this small-α limit. The leading-order dynamics only involve an interaction between the salinity concentration and the stream function. The only rôle that temperature plays is in the setting up of the background salinity and velocity fields. This lack of a rôle for the temperature perturbation is not due to the very different salt and heat diffusivities as no such assumption has been made in this small-α analysis. The no-flux boundary conditions imposed on the salt concentration allow large concentration variations to build up. These concentration perturbations are essentially uniform across the slot and so can only decay by diffusion in the vertical direction with an associated long time scale. Since the temperature perturbation is zero at the walls the time scale for its dissipation is the diffusion time across the slot
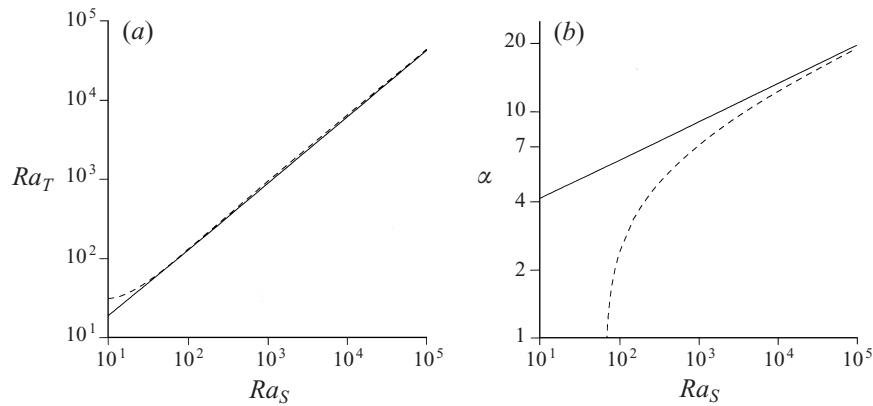
FIGURE 7. A comparison of the asymptotic behaviour (solid line) and the full numerical calculations (dashed line) for the large-Ra_S limit: (*a*) the critical value of Ra_T and (*b*) the corresponding vertical wavenumber, α.

width, which is a much faster scale. If, however, different boundary conditions were imposed on the salinity, its concentration would vary across the slot at leading-order and so it too would diffuse on a time scale based on the slot width. This is a much shorter time scale and would significantly alter the above analysis.

3.4. *Large salinity gradient*

The leading-order asymptotic behaviour of this region (numbered 4 in figure 1) was first investigated by Thorpe *et al.* (1969). This analysis was extended by Hart (1971) who considered the higher-order effects of the boundary layers at the walls. The leading-order condition for marginal stability in this region is

$$Ra_T(\tau^{-1} - 1) = 3^{1/2}(2\pi)^{2/3}(Ra_S/\tau)^{5/6} \qquad (3.32a)$$

with

$$\alpha = (\pi^2/2)^{1/6}(Ra_S/\tau)^{1/6}. \qquad (3.32b)$$

A comparison of these results with the full numerical results is shown in figure 7. The agreement between the critical thermal Rayleigh number and the asymptotic estimate is remarkable close down to around $Ra_S = 30$. This is entirely fortuitous as at this low level the small-α asymptotics of the previous subsection is the appropriate regime. The large-Ra_S assumption is equivalent to assuming that α is large, which obviously cannot be the case if α is assumed to be small. As Ra_S increases there is a slight divergence of the asymptotic result and the full numerical result. This difference decreases as Ra_S increases. A more realistic impression of the convergence of the full solution to the large-Ra_S asymptotic regime can be seen by comparing the wavenumbers for the full solutions with their asymptotic limit. This is shown in figure 7(*b*). Here the two lines gradually converge as Ra_S increases.

In this region the instabilities take the form of thin almost horizontal layers whose vertical scale is given by the Chen scale (Chen, Briggs & Wirtz 1971), which in dimensional terms is $h = (\alpha \Delta T)/(-\overline{S}_z)$. As the convective instabilities in this regime are constrained by this Chen scale in the vertical direction and the slot width in the horizontal direction we can use the mechanistic argument of Kerr (1989). This argument was applied to the double-diffusive convection that occurs when a salinity gradient is heated from a single vertical wall, but it will also apply equally here.
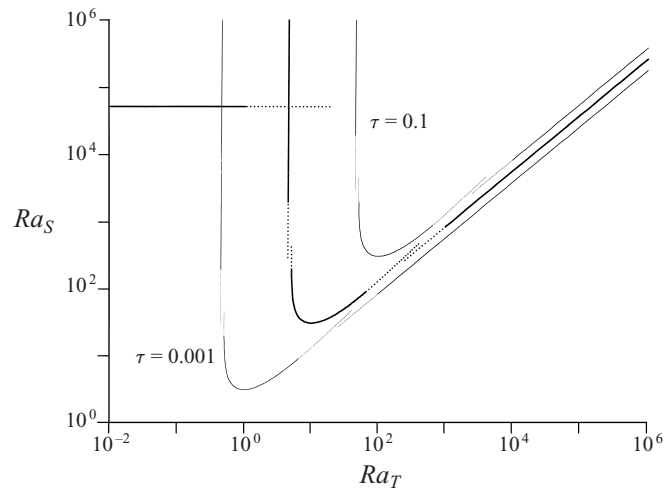
FIGURE 8. A schematic diagram showing the four different leading-order asymptotic regimes examined here for $\sigma = 6.7$ and $\tau = 0.01$ (heavy lines). The position of the horizontal line at the left is a function of the Prandtl number, σ. The other three lines move together in the diagonal direction as the salt/heat diffusivity, τ varies. The positions for $\tau = 0.1$ and $\tau = 0.001$ are shown by the thin lines. The oscillatory branch of instabilities is not shown.

This argument indicates that the natural non-dimensional parameter that governs the instabilities in this regime is

$$Q = \frac{(1-\tau)^6 g(\alpha \Delta T)^6}{\nu \kappa_S D^2 \left(-\beta \overline{S}_z\right)^5}. \tag{3.33}$$

This parameter is related to a Rayleigh number but involves two lengthscales: the width of the slot and the vertical Chen scale. Instability in a slot occurs when this parameter exceeds $432\pi^4$, which is equivalent to the above result of Thorpe *et al.* and Hart. Kerr went on to find the next-order perturbation of Q for the case of heating a salinity gradient at an isolated vertical wall. The appropriate expansion parameter was the square of the ratio of the Chen scale to the horizontal length scale, with an extra factor of $(1 - \tau)$. In the variables used here this is $((1 - \tau)Ra_T/Ra_S)^2$. At the right-hand end of the graphs in figure 6 this quantity has only just gone below 0.2, and so the agreement is well within reasonable expectations.

In this region the length scale for the diffusion of both the temperature and the salinity perturbations is the same: the Chen scale. Hence both T and S are involved in the leading-order behaviour.

4. Discussion

The stability boundaries derived from the four asymptotic regimes described in this paper are shown schematically by the heavy lines in figure 8 for Prandtl number $\sigma = 6.7$ and salt/heat diffusivity ratio $\tau = 0.01$. The solid lines show the regions where the asymptotic regimes are appropriate, and the dotted lines show their continuations. If these regions are joined by reasonably simple curves then just about all of the full stability boundary in figure 1 is recovered. The only portion that would be missing is the portion where the primary mode of instability is oscillatory.

The results of the four asymptotic analyses of the previous Section fall into two

categories. The first, the small-Ra_S limit, gives a leading-order result which is that for convection in an unstratified slot, and takes the form $Ra_T = f(\sigma) \approx 7880\sigma$ (Vest & Arpaci 1969) for $\sigma < 12.7$. For larger values of the Prandtl number the values of the critical thermal Rayleigh number, Ra_T, have a more complicated dependence on the Prandtl number which cannot be shown clearly on this schematic diagram. The position of this portion of the stability boundary is determined by the Prandtl number alone to leading-order. The other three asymptotic results fall into the second category which has the common property that in the limit $\tau \to 0$ (a limit appropriate for most salts in most fluids) they can all be express in the form

$$G\left(Ra_T/\tau, Ra_S/\tau\right) = 0. \tag{4.1}$$

Thus the positions of these portions of the boundaries are determined by the salt/heat diffusivity ratio alone. Another important consequence is that the relative positions of these three asymptotic regimes in the $(\log Ra_T, \log Ra_S)$-plane is fixed. These portions of the stability boundary move around as a unit along a diagonal of slope 1 as τ varies. This is illustrated in figure 8 where the positions of the stability boundaries given by these three asymptotic regimes are also shown by the light lines for $\tau = 0.1$ and $\tau = 0.001$. Thus the general features of the stability boundary for non-oscillatory instabilities in a vertical slot are known for most practical situations where τ is small. The oscillatory branch of solutions only occupies a restricted region of the stability curve for the case of water and common salt covered here. Young & Rosner (1998) found the oscillatory part of the stability boundary for some other values of τ; its size did not seem to vary much with these changes in parameters. This oscillatory regime does not seem to lend itself to an asymptotic analysis which would allow a description of its stability boundary for general σ and τ in the way that the other regimes do.

The shape of the marginal stability curve tells us that for any given solute there are two important conditions for the onset of instabilities. First, is the salinity stratification strong enough? And secondly, is the temperature difference strong enough? As τ gets smaller both these conditions become less stringent. For example, if the solute was a protein instead of common salt then τ could be reduced by a factor of 100, and so the temperature difference across the walls of a container that could initiate convection would be 100 less than that required to start convection with the stratification due to common salt, and well over 100 000 times less than is required to cause cellular convection in the absence of any solute stratification. With the minimum temperature difference required to cause convection in a protein solution being less than $10^{-4}\,^\circ$C in a 1 cm wide slot, it may be very hard *not* to have convection in the presence of any stratification.

The importance of the portion of the stability boundary covered by the large-temperature-difference asymptotics may seem a bit obscure at first. After all, it only applies to one precise salinity gradient. However, in practice it takes some time for heat to diffuse across a slot and a linear horizontal temperature gradient to be established. If the wall temperature is raised quickly then the effective instantaneous Rayleigh numbers will be governed by the distance that the heat has diffused into the fluid and not the slot width. Thus Ra_T will grow like $t^{3/2}$ and Ra_S like t^2. These instantaneous Rayleigh numbers may well evolve towards their final state in such a way as to cross this asymptotic boundary. The exact details of the behaviour on this boundary will not be applicable for such an evolving system, but it may give a qualitative indication of the behaviour that may be expected. Similarly this may give an indication of some of the expected behaviour in experiments where a salinity gradient is heated rapidly from a single vertical boundary. In Tanny & Tsinober (1988) the evolving salt and

thermal Rayleigh numbers were traced in their single boundary experiments. The values of these at the onset of instability are consistent with a stability boundary whose shape is similar to that of a vertical slot. The theory for the rapid heating of a single boundary is not well understood (Kerr 1996). However, the observation that these instabilities are driven by the horizontal salinity gradients and stabilized by the shear may give an insight into the first appearance of instabilities. The presence of transient vertical motions near the heated wall was clearly shown by Schladow, Thomas & Koseff (1992) and the onset of instabilities could be associated with times when these initial velocities reduce in magnitude.

One aspect of this analysis that could impose limitations on its applicability is the assumption of a steady state in an infinite channel. In practical situations there will be ends to the channel, and these will have an effect. Upper and lower boundaries that are impermeable will result in a background state which is evolving with time even without an applied temperature difference, although the low diffusivity of salt does mean that time for disturbances to diffuse from the endwalls is long. However, the end regions of the slot will always present a difficulty, both analytically and experimentally. The analysis presented here should be a useful guide to what happens in the core of a vertical cavity where the end effects are not strongly felt. Another possible problem with finite cavities is the restriction on the vertical wavenumber of instabilities. The limit $\alpha \to 0$ implies disturbances of unbounded height. The heating required to initiate convection in cells of small but finite wavenumber is close to that found in the small-α limit. Near to marginal stability only a few tall convection cells may be observed in the slot.

The difference between our results, and those of Young & Rosner, and the original results of Thangam *et al.* may well be due to the insufficient resolution used in their original calculations for some regions of the marginal stability curve. One of the strengths of the Galerkin approach is that it can produce solutions to difficult problems. Its drawback is that it can produce plausible incorrect solutions. The different numerical results obtained here have been confirmed by the use of independent numerical methods and asymptotic analysis.

Appendix

Here we find an approximation to the solution, S_0, of the salinity equation

$$\left(\frac{\mathrm{d}^2}{\mathrm{d}x^2} - \alpha^2\right) S_0 + \frac{\mathrm{i}\alpha\psi_0 Ra_{T0}\overline{S}'_0(x)}{\tau} - \frac{\mathrm{i}\alpha Ra_{T0}\overline{W}_0(x)}{\tau} S_0 + \psi'_0/\tau = 0, \qquad (A\,1)$$

where ψ_0 is a given function of x. We can write this in more general terms as

$$S''_0 - (\alpha^2 + \mathrm{i}\mu x(x^2 - \tfrac{1}{4}))S_0 = f(x) \qquad (A\,2)$$

where μ is assumed to be large, α is $O(1)$ and $f(x)$ some known function of x. The boundary conditions are $S'_0(\pm\tfrac{1}{2}) = 0$. If x is not small, or near $\pm\tfrac{1}{2}$, then we get the outer behaviour

$$S_o(x) \sim -\frac{f(x)}{\mathrm{i}\mu x(x^2 - \tfrac{1}{4})}. \qquad (A\,3)$$

When x is small or near $\pm\tfrac{1}{2}$ this approximation breaks down. Near $x = 0$ the appropriate length scale for the problem is $X = \mu^{1/3}x$. Using this scale gives the
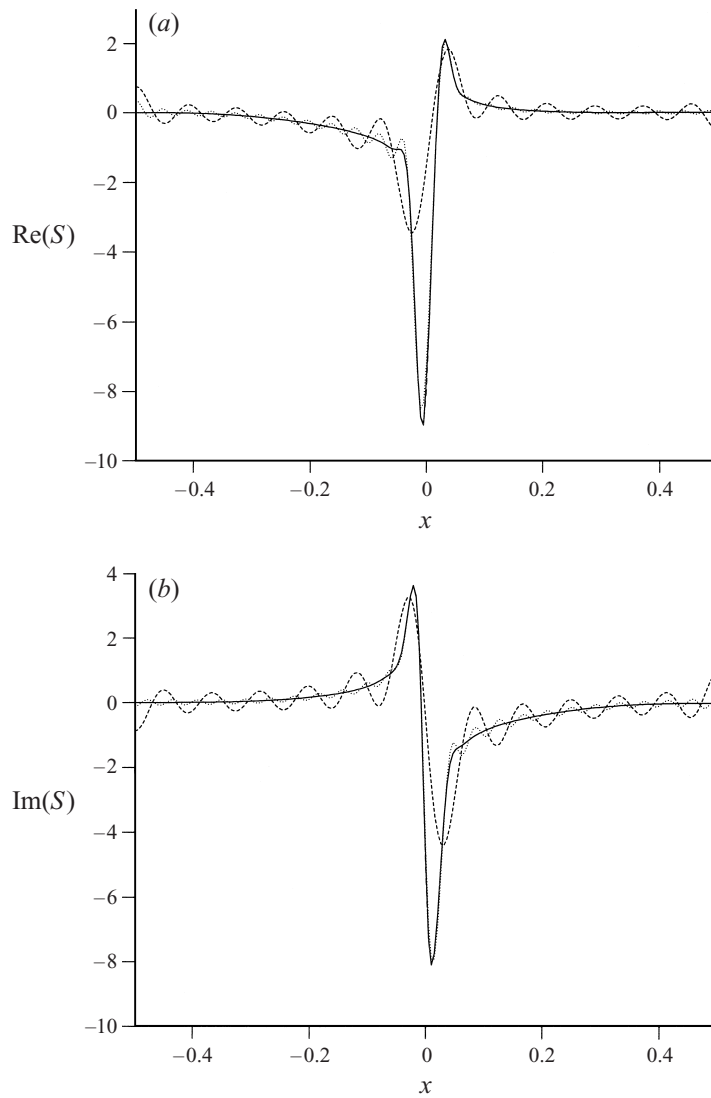
FIGURE 9. A comparison of (*a*) the real and (*b*) imaginary parts of the asymptotic solution to the salinity equation in the small-Ra_S limit (solid line) with the solutions calculated with truncation levels of $N = 24$, 48 and 96 for $Ra_S = 0.001$. The line for $N = 24$ is dashed and for $N = 48$ dotted. A dashed line for the results with $N = 96$ is also plotted, but is barely distinguishable from the solid line of the asymptotics.

leading-order inner problem

$$\frac{\mathrm{d}^2 S_i}{\mathrm{d}X^2} + \mathrm{i}X S_i = \mu^{-2/3} f(0). \tag{A 4}$$

The solution that is required is one that decays for $X \to \pm\infty$. This leading-order problem does not have an exact solution if $f(0)$ is non-zero as is the case here. It has to be evaluated numerically, but this is straightforward.

Once both the inner solution, $S_i(X)$, and the outer solution, $S_o(x)$, are known a

composite expansion can be written down:

$$S_0(x) \sim S_i(\mu^{-1/3}x) + S_o(x) + \frac{4f(0)}{i\mu x}. \qquad (A\,5)$$

This will be valid to leading-order everywhere except at $x = 0$ where the value $S_i(0)$ is taken, and in the boundary layers near $x = \pm\frac{1}{2}$. These boundary layers can be treated in a similar way, but since the boundary conditions on $\psi_0(x)$ and $\psi_0'(x)$ at the walls requires $f(x)$ to decay to 0, these regions do not play a significant rôle in the integrations required to find Ra_{T1} in §3.1, and so these calculations are omitted. A comparison between this estimate of the the solution $S_0(x)$ compared to that calculated for the full numerical problem using the Galerkin approach with $N = 96$, 48 and 24 for $Ra_S = 0.001$ is shown in figure 9. The results for the asymptotic estimate and the numerical solution for $N = 96$ are almost indistinguishable, while the results for $N = 48$ and $N = 24$ show significant differences. In particular the result for $N = 24$ fails to resolve the sharp peak seen near $x = 0$. This peak is a major part of the salinity perturbation, and makes a significant contribution to the integral (3.10). Any truncation that failed to resolve this peak would provide unreliable numerical results.

REFERENCES

BATCHELOR, G. K. 1954 Heat transfer by free convection across a closed cavity between vertical boundaries at different temperatures. *Q. J. Appl. Maths* **12**, 209–233.

BRANDT, A. & FERNANDO, H. J. S. 1996 *Double-Diffusive Convection.* American Geophysical Union.

CHEN, C. F., BRIGGS, R. A. & WIRTZ, D. G. 1971 Stability of thermal convection in a salinity gradient due to lateral heating. *Intl J. Heat Mass Transfer* **14**, 57–65.

HART, J. E. 1971 On sideways diffusive instability. *J. Fluid Mech.* **49**, 279–288.

HART, J. E. 1973 Finite amplitude sideways diffusive convection. *J. Fluid Mech.* **59**, 47–64.

KERR, O. S. 1989 Heating a salinity gradient from a vertical sidewall: linear theory. *J. Fluid Mech.* **207**, 323–352.

KERR, O. S. 1996 Double-diffusive instabilities at a vertical boundary. In *Double Diffusive Convection* (ed. A. Brandt & J. Fernando), pp. 105–113. American Geophysical Union.

KORPELA, S. A., GÖZÜM, D. & BAXI, C. B. 1973 On the stability of the conduction regime of natural convection in a vertical slot. *Intl J. Heat Mass Transfer* **16**, 1683–1690.

LINDEN, P. F. 1974 Salt fingers in a steady shear flow. *Geophys. Fluid Dyn.* **6**, 1–27.

SCHLADOW, S. G., THOMAS, E. & KOSEFF, J. R. 1992 The dynamics of intrusions into a thermohaline stratification. *J. Fluid Mech.* **236**, 127–165.

STERN, M. E. 1960 The 'salt fountain' and thermohaline convection. *Tellus* **12**, 172–175.

STERN, M. E. 1967 Lateral mixing of water masses. *Deep-Sea Res.* **14**, 747–753.

STOMMEL, H., ARONS, A. B. & BLANCHARD, D. 1956 An oceanographical curiosity: the perpetual salt fountain. *Deep-Sea Res.* **3**, 152–153.

TANNY, J. & TSINOBER, A. B. 1988 The dynamics and structure of double-diffusive layers in sidewall-heating experiments. *J. Fluid Mech.* **196**, 135–156.

THANGAM, S., ZEBIB, A. & CHEN, C. F. 1981 Transition from shear to sideways diffusive instability in a vertical slot. *J. Fluid Mech.* **112**, 151–160.

THORPE, S. A., HUTT, P. K. & SOULSBY, R. 1969 The effects of horizontal gradients on thermohaline convection. *J. Fluid Mech.* **38**, 375–400.

VEST, C. M. & ARPACI, V. A. 1969 Stability of natural convection in a vertical slot. *J. Fluid Mech.* **36**, 1–15.

YOUNG, Y. & ROSNER, R. 1998 Linear and weakly nonlinear analysis of doubly-diffusive vertical slot convection. *Phys. Rev.* E **57**, 5554–5563.